

Analysis and Development of a Disturbance Compensation Approach for Performance Improvement in Speed Control

Ke-Han Su*, Ming-Yang Cheng**, and Jen-Che Wu **

Keywords: Disturbance compensation; Load torque; Friction force; Low-speed; Motion control

ABSTRACT

In high-precision motion control applications, elimination of adverse effects caused by friction and disturbance is a key issue. In particular, when the system undergoes low-speed or reversal motions, the inherent friction force and/or external disturbances may degrade motion accuracy. Therefore, in order to achieve satisfactory motion accuracy, it is necessary to suppress the adverse effects due to friction and/or disturbance. In order to deal with the aforementioned problem often encountered in motion control applications, this paper develops a disturbance compensation approach, which is called Nominal-plant-based Disturbance Compensator (NDC). The advantage of the proposed NDC is that it not only can accurately estimate external disturbance/load torque, but also has superior ability in external disturbance suppression and measurement noise reduction. To address the properties of the proposed approach, theoretical analysis of the transfer functions for different schemes are derived first. Subsequently, several experiments on load torque estimation, speed control, and contour are conducted to evaluate the performance of the proposed approach. Experimental results demonstrate the effectiveness of the proposed approach.

1. INTRODUCTION

Nowadays, high-performance servo-mechanisms such as micro motion stages, industrial manipulators, and Computer Numerical Control (CNC) machine tools are required to perform highly precise motion control (Su & Cheng, 2008). However, in such control applications, motion accuracy and

performance control applications, motion accuracy and performance may deteriorate due to unknown system uncertainties or nonlinearities. For instance, when a servomechanism is operated under a low-speed or reversal motion, the inherent friction force often causes a stick-slip phenomenon that will ultimately degrade the motion accuracy. In addition, external disturbances such as external load or cutting forces may also degrade the motion performance. To cope with the above difficulties, there are many studies focusing on developing different control strategies to improve the motion accuracy. Among the existing conventional control schemes, the feedback control technique is widely used to deal with problems due to external disturbances and friction force in a motion control system (Tomizuka, 1993; Tarn & Cheng, 1995). For instance, Tarn and Cheng (1995) employed an appropriate gain tuning strategy for a PID controller to overcome the friction effects encountered in contour-following tasks of CNC machine tools. In addition to the conventional feedback control scheme, many different friction models such as the LuGre friction model, have been developed so as to eliminate the friction effects (Karnopp, 1985; Canudas de Wit et al., 1995).

On the other hand, to deal with issues such as external disturbance or parameter variation /uncertainty, the disturbance observer (DOB) is one of the most popular and easily implemented approaches for disturbance estimation/suppression in motion control problems. Over the past decades, several investigations on different types of disturbance observer/compensator have been proposed in many servo control applications (Ohishi et al., 1987; Ko et al., 1993; Umeno & Hori, 1991; Choi et al., 1999; Tsai et al., 2000). Firstly, some researchers regard the external disturbance (e.g., load torque) as an augmented state variable so that the linear system theory is exploited to estimate the external load torque for disturbance suppression (Ohishi et al., 1987; Ko et al., 1993). In this type of disturbance observer, the external disturbance is commonly assumed to be a constant. On the contrary, other researchers regard the difference between the command input and the calculated input (which is obtained through an inverse nominal model) as an

Paper Received January, 2021. Revised April, 2021. Accepted May, 2021. Author for Correspondence: Ke-Han Su

* Department of Electrical Engineering, National Yunlin University of Science & Technology, Yunlin, 640301, Taiwan

** Department of Electrical Engineering, National Cheng Kung University, Tainan, 701, Taiwan

equivalent disturbance, in which it is used as a feedback signal to eliminate external disturbances (Umeno & Hori, 1991). Similarly in Choi et al. (1999) and Tsai et al. (2000), based on the difference between the output of the real plant and the output of the identified nominal model, a model reference-based disturbance observer was also developed for external disturbances estimation/elimination.

Recently, several extended investigations have been proposed to further improve the performance of disturbance estimation/suppression (Umeno & Hori, 1991; Lee & Tomizuka, 1996; Kobayashi et al., 2007; Lu, 2008; Yao et al., 1997; Kim & Chung, 2003; Xie, 2010, Shao et al. 2021). For instance, Umeno and Hori (1991), Lee and Tomizuka (1996), Kobayashi et al. (2007), and Lu (2008) designed different types of low-pass filters for performance improvement of DOB. Generally, the disturbance observer is designed based on the linear system theory. Therefore, the effectiveness of DOB may deteriorate when used in practical applications where significant parameter variations and/or nonlinear uncertainties often occur. To deal with such problems, Kobayashi et al. (2007) developed a phase compensation scheme based on a disturbance observer which considers the issue of inertia variations. In addition, to further cope with the effects of discontinuous disturbances and large parameter variations, Yao et al. (1997) developed an adaptive robust control (ARC) scheme consisting of a model reference-based disturbance observer, a sliding mode control, and an adaptive control scheme. Moreover, by employing robust internal-loop compensator (RIC), Kim and Chung (2003) proposed an advanced design method to further enhance the robustness of DOB. Furthermore, in addition to the use of a model-based disturbance observer in dealing with external disturbances, Xie (2010) also developed a compensation scheme for measurement noise rejection.

In this paper, a disturbance compensation approach called the Nominal-plant-based Disturbance Compensator (NDC) is proposed to deal with the speed control problem for a motion control system. Basically, the concept of NDC is similar to the model reference-based disturbance observer which is exploited to obtain the difference between the output of the identified nominal model and the output of the real plant. After calculating the difference, the estimated disturbances can be obtained via a PI type compensator and then fed back to the real plant to suppress external disturbances. Moreover, to eliminate the measurement noise effects, instead of using the real motor velocity, the velocity information obtained from the nominal plant model is used as the velocity feedback signal.

The rest of the paper is organized as follows. Section 2 consists of a brief introduction and analysis to the conventional disturbance observer and the PI-type Close-loop Torque Observer (PICTO). Theoretical analysis of the compensation capability of the

PICTO used in disturbance compensation is also provided. Detailed analysis of the proposed NDC is given in Section 3. Section 4 contains the experimental setup and results. Finally, the conclusions are summarized in Section 5.

2. DISTURBANCE OBSERVER FOR MOTION CONTROL SYSTEMS

2.1 Brief Introduction to the disturbance observer (DOB)

In precision motion applications, external disturbance and load torque often present a great challenge to control designers since they deteriorate motion accuracy. One of the most commonly used approaches to circumvent their influence is to use a suitable sensor to measure their amount. Based on the measured value, one can design a suitable compensator to improve motion accuracy. However, sensors are not always available for all application scenarios. Even if they are available, they may not be cost-effective. In order to overcome this difficulty, Ohishi et al. (1987) exploited the linear system theory to design an observer that can be used to estimate external disturbances and load torque. Extending the concept of the disturbance observer, Umeno and Hori (1991) developed a robust speed controller and a Butterworth low-pass filter which is based on the parameterized formula. Recently, this type of DOB has become a well-known and useful approach for external disturbance estimation and compensation in motion control (Lee & Tomizuka, 1996, Sariyildiz et al. 2020). Generally, the main advantage of DOB is that it can accurately estimate external disturbance and compensate for it without changing the existing control paradigm. However, there exists a derivative term in the DOB structure which may introduce high frequency noise. In order to overcome this difficulty, one needs to design a low-pass filter and also adjust the bandwidth of DOB. In the following, theoretical analysis of the conventional DOB will be conducted to verify its capability in disturbance estimation.

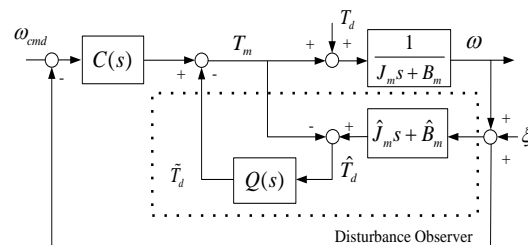


Fig. 1 Block diagram of a motion control system with a disturbance observer.

Figure. 1 illustrates the schematic diagram of the disturbance observer used in speed control of a motion control system. In Fig.1, the dotted line rectangle is the structure of DOB developed by Umeno and Hori (1991), where $1/(J_m s + B_m)$ represents the real transfer function of the plant under control, $\hat{J}_m s + \hat{B}_m$ represents the inverse of the identified nominal model, ξ is

the measurement noise, $Q(s)$ is the low-pass filter, $C(s)$ is the speed controller (e.g. a PI-type controller), and ω_{cmd} and ω are the velocity command and output velocity, respectively. T_m , T_d , \hat{T}_d , and \tilde{T}_d are the torque command, real load torque, estimated load torque, and calculated load torque difference.

Note that \tilde{T}_d is the difference between the input of the real plant and the output of the identified nominal model. By using the Mason's gain formula (Nise, 2007), the transfer function from the torque command to the estimated load torque in Fig.1 is expressed as:

$$\frac{\tilde{T}_d(s)}{T_m(s)} = \frac{Q(s)((\hat{J}_m s + \hat{B}_m) - (J_m s + B_m))}{(J_m s + B_m) + Q(s)((\hat{J}_m s + \hat{B}_m) - (J_m s + B_m))} \quad (1)$$

Similarly, the transfer function from the real load torque to the estimated load torque is expressed as:

$$\frac{\tilde{T}_d(s)}{T_d(s)} = \frac{Q(s)(\hat{J}_m s + \hat{B}_m)}{(J_m s + B_m) + Q(s)((\hat{J}_m s + \hat{B}_m) - (J_m s + B_m))} \quad (2)$$

For the sake of easy analysis, without loss of generality, the torque command and load torque are set to constant values in the following derivations. That is, $T_m(s) = C_m/s$, $T_d(s) = C_d/s$, where C_m and C_d are constant. In addition, the low-pass filter and the measurement noise are set as $Q(s) = 1$ and $\xi = 0$, respectively. Therefore, Eq. (1) and Eq. (2) can be further rewritten as follows:

$$\tilde{T}_{dm}(s) = \frac{(\hat{J}_m s + \hat{B}_m) - (J_m s + B_m)}{(J_m s + B_m) + ((\hat{J}_m s + \hat{B}_m) - (J_m s + B_m))} \times \frac{C_m(s)}{s} \quad (3)$$

$$\tilde{T}_{dd}(s) = \frac{(\hat{J}_m s + \hat{B}_m)}{(J_m s + B_m) + ((\hat{J}_m s + \hat{B}_m) - (J_m s + B_m))} \times \frac{C_d(s)}{s} \quad (4)$$

By letting $s \rightarrow 0$ in Eq. (3) and Eq. (4), it is easy to find that in steady state, the estimated load torque due to the torque command and the real load torque can be described by Eq. (5) and Eq. (6), respectively.

$$\tilde{T}_{dm}(s) = \frac{\hat{B}_m - B_m}{\hat{B}_m} \times C_m \quad (5)$$

$$\tilde{T}_{dd}(s) = \frac{\hat{B}_m}{\hat{B}_m} \times C_d \quad (6)$$

In addition, by accounting for all the estimated load torque obtained from Eq. (5) and Eq. (6), the overall estimated load torque \tilde{T}_{dss} in steady state can be rewritten as:

$$\tilde{T}_{dss} = \tilde{T}_{dm} + \tilde{T}_{dd} = \frac{\hat{B}_m - B_m}{\hat{B}_m} \times C_m + \frac{\hat{B}_m}{\hat{B}_m} \times C_d \quad (7)$$

If the identified nominal model is accurate enough (i.e. $\hat{B}_m \cong B_m$), Eq. (7) can be simplified as $\tilde{T}_{dss} \cong C_d$. It indicates that the conventional DOB has good disturbance estimation ability. However, the estimation performance of DOB is limited by the bandwidth of the low-pass filter. In other words, if the type of the low-pass filter is chosen properly, the equivalent load torque used to compensate for the real load torque can be accurately computed and the measurement noise can also be effectively suppressed. Selection suggestions for the type of low-pass filter for the disturbance observer can be found in Umeno and Hori (1991).

2.2. PI-type Close-loop Torque Observer (PICTO)

As previously mentioned, there are many studies focusing on developing disturbance observers for load torque/disturbances estimation. PICTO is one of those approaches (Tsai et al., 2000). Figure 2 illustrates the block diagram of a speed control system with a PICTO. In Fig. 2, $\frac{1}{(J_m s + B_m)}$ represents the real transfer function of the plant under control, while $\frac{1}{(\hat{J}_m s + \hat{B}_m)}$ represents the nominal plant model obtained through system identification. Also in Fig. 2, T_m , T_d , and \hat{T}_d are the torque command, real load torque, and the load torque estimated from the PICTO. ω_{cmd} , ω , and $\hat{\omega}$ are the velocity command, velocity of the real plant, and the output of the identified nominal model, respectively. In addition, K_p and K_i are the proportional and integral gains of the velocity loop controller, while K_1 and K_2 are the gain constants used to adjust the pole position of the disturbance observer (Tsai et al., 2000; Wu et al., 2010). To analyze the ability of disturbance estimation of the PICTO, similarly, by using the Mason's gain formula, the transfer function from the torque command to the estimated load torque in Fig.2 is expressed as:

$$\frac{\hat{T}_d(s)}{T_m(s)} = \frac{(K_1 s + K_2)((J_m s + B_m) - (\hat{J}_m s + \hat{B}_m))}{(J_m s + B_m)(\hat{J}_m s^2 + \hat{B}_m s + K_1 s + K_2)} \quad (8)$$

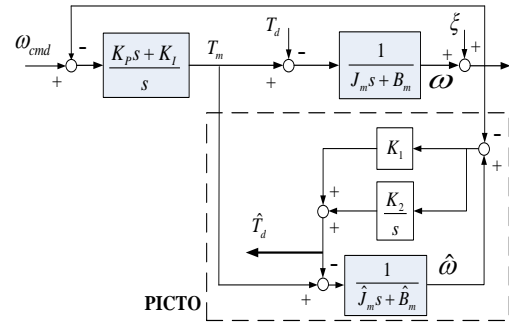


Fig. 2 Block diagram of a speed control system with the PICTO.

Also, the transfer function from the real load torque to the estimated load torque is expressed as:

$$\frac{\hat{T}_d(s)}{T_d(s)} = \frac{(\hat{J}_m s + \hat{B}_m)(K_1 s + K_2)}{(J_m s + B_m)(\hat{J}_m s^2 + \hat{B}_m s + K_1 s + K_2)} \quad (9)$$

To facilitate the analysis, without loss of generality, under the same assumption used in the previous subsection, Eq.(8) and Eq.(9) can be further rewritten as Eq. (10) and Eq. (11), respectively:

$$\hat{T}_{dm}(s) = \frac{(K_1 s + K_2)((J_m s + B_m) - (\hat{J}_m s + \hat{B}_m))}{(J_m s + B_m)(\hat{J}_m s^2 + \hat{B}_m s + K_1 s + K_2)} \times \frac{C_m(s)}{s} \quad (10)$$

$$\hat{T}_{dd}(s) = \frac{(\hat{J}_m s + \hat{B}_m)(K_1 s + K_2)}{(J_m s + B_m)(\hat{J}_m s^2 + \hat{B}_m s + K_1 s + K_2)} \times \frac{C_d(s)}{s} \quad (11)$$

By letting $s \rightarrow 0$ in Eq. (10) and Eq. (11), it is easy to find that in steady state, the overall estimated load torque \hat{T}_{dss} can be rewritten as:

$$\hat{T}_{dss} = \hat{T}_{dm} + \hat{T}_{dd} = \frac{K_2(B_m - \hat{B}_m)}{B_m K_2} \times C_m + \frac{\hat{B}_m K_2}{B_m K_2} \times C_d \quad (12)$$

Similarly, if the nominal plant model obtained from system identification is accurate enough, one will

have $B_m \cong \hat{B}_m$. Thus, Eq. (12) can be further simplified as $\hat{T}_{dss} \cong C_d$. Obviously, it indicates that the estimated load torque obtained from the PICTO gives a good approximation of the real load torque.

2.3. Disturbance Compensation Using the PICTO

Theoretical analysis conducted in the previous subsection shows that the PICTO is effective in estimating external disturbance. Nevertheless, its ability in compensating for the external disturbance may suffer from the fact that an additional feedback loop is generated (with the bold compensation path as shown in Fig. 3). To validate this viewpoint, similar analyses of estimation ability in disturbance compensation using the PICTO are given in the following. Figure 3 illustrates the block diagram of the disturbance compensation structure with the PICTO (as indicated in the dashed line rectangle) in a motion control system.

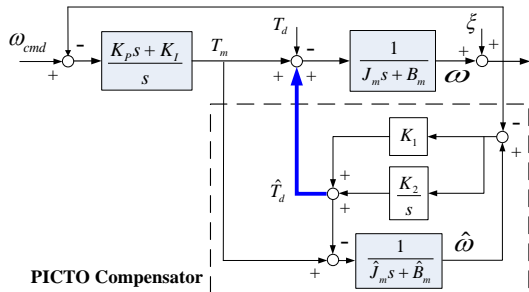


Fig. 3 Block diagram of the disturbance compensation structure using the PICTO.

Similarly, using the Mason’s gain formula, the transfer functions from the torque command to the estimated load torque and from the real load torque to the estimated load torque in Fig.3 are expressed as:

$$\frac{\hat{T}_d(s)}{T_m(s)} = \frac{(K_1s + K_2)((J_m s + B_m) - (\hat{J}_m s + \hat{B}_m))}{(\hat{J}_m s + \hat{B}_m)(J_m s + B_m)s + (K_1s + K_2)((\hat{J}_m s + \hat{B}_m) + (J_m s + B_m))} \quad (13)$$

$$\frac{\hat{T}_d(s)}{T_d(s)} = \frac{(K_1s + K_2)(\hat{J}_m s + \hat{B}_m)}{(\hat{J}_m s + \hat{B}_m)(J_m s + B_m)s + (K_1s + K_2)((\hat{J}_m s + \hat{B}_m) + (J_m s + B_m))} \quad (14)$$

Therefore, under the same assumption used in the previous subsections, the overall estimated external load torque \hat{T}_{dss} in the steady state can be further rewritten as:

$$\hat{T}_{dss}(s) = \hat{T}_{dm}(s) + \hat{T}_{dd}(s) = \frac{K_2(B_m - \hat{B}_m)}{K_2(B_m + \hat{B}_m)} \times C_m + \frac{K_2 \hat{B}_m}{K_2(B_m + \hat{B}_m)} \times C_d \quad (15)$$

Additionally, if the nominal plant model is accurate enough, Eq. (15) can be simplified as $\hat{T}_{dss} \cong C_d/2$. In other words, the estimated external load torque is only half of the real load torque when the PICTO is used in disturbance compensation.

3. THE PROPOSED NOMINAL-PLANT-BASED DISTURBANCE COMPENSATOR

As previously mentioned in subsection 2.3, the estimation performance may deteriorate if the PICTO is used in disturbance compensation in a motion control system. To ease this problem, this paper develops an alternative disturbance estimation /compensation approach, which is called Nominal-plant-based Disturbance Compensator (NDC). The idea and analysis of the proposed NDC are elaborated upon in this subsection.

The schematic diagram of a speed control system with the proposed NDC is illustrated in Fig. 4, where $K_P, K_I, \omega_{cmd}, \omega, \hat{\omega}, T_m, T_d, \hat{T}_d, \zeta, K_1, K_2, J_m, B_m, \hat{J}_m$, and \hat{B}_m have been defined in Section 2. Compared with the disturbance compensation structure based on the PICTO shown in Fig. 3, two paths have been modified in the proposed NDC. Firstly, in order to obtain accurate disturbance estimation, the path from the estimated disturbance to the nominal-plant model is eliminated. In addition, to further suppress the noise effects, instead of using the velocity of the real plant, the velocity information obtained from the nominal-plant model is adopted as the feedback signal. Detailed descriptions and analysis of the proposed NDC is provided in the following.

Similar to the discussions in previous subsections, the transfer functions from the torque command to the estimated load torque and from the real load torque to the estimated load torque in Fig.4 can be described by Eq. (16) and Eq.(17), respectively.

$$\frac{\hat{T}_d(s)}{T_m(s)} = \frac{(K_1s + K_2)((J_m s + B_m) - (\hat{J}_m s + \hat{B}_m))}{(\hat{J}_m s + \hat{B}_m)((J_m s + B_m)s + (K_1s + K_2))} \quad (16)$$

$$\frac{\hat{T}_d(s)}{T_d(s)} = \frac{(K_1s + K_2)}{(J_m s + B_m)s + (K_1s + K_2)} \quad (17)$$

In addition, under the same assumption used in previous subsections, the overall estimated load torque \hat{T}_{dss} in the steady state can be further rewritten as:

$$\hat{T}_{dss}(s) = \hat{T}_{dm}(s) + \hat{T}_{dd}(s) = \frac{K_2(B_m - \hat{B}_m)}{K_2 \hat{B}_m} \times C_m + \frac{K_2}{K_2} \times C_d \quad (18)$$

Suppose that the identified nominal plant model is accurate enough. This is to say, that Eq. (18) can be easily simplified as $\hat{T}_{dss} \cong C_d$. Clearly, it indicates that the estimated load torque obtained using the NDC is equal to the real load torque. Theoretical analysis suggests that the proposed NDC can provide accurate disturbance estimation when used in disturbance elimination for motion control systems.

On the other hand, as shown in Fig. 4, there is no path from the measurement noise ζ to the output of the nominal plant model $\hat{\omega}$. Therefore, the transfer function from ζ to $\hat{\omega}$ can be expressed as:

$$\frac{\hat{\omega}}{\zeta} = \frac{0}{\Delta} \quad (19)$$

$$\Delta = (\hat{J}_m s + \hat{B}_m)(J_m s + B_m)s^2 + (K_p s + K_i)(J_m s + B_m)s + (K_1s + K_2)(\hat{J}_m s + \hat{B}_m)s + (K_p s + K_i)(K_1s + K_2) \quad (20)$$

Clearly, Eq. (20) reveals that the measurement noise does not have any effect on the output of the nominal-plant model in the proposed NDC. According to the above discussions, one can conclude that the proposed approach can effectively compensate for the load torque even in a scenario where the measurement noise exists.

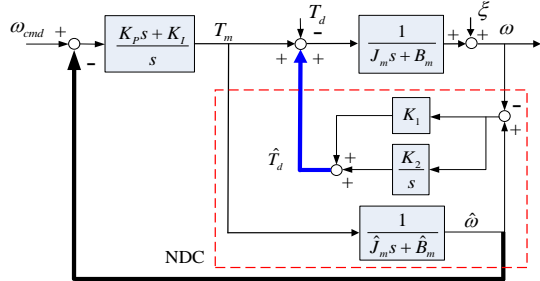


Fig. 4 Block diagram of a speed control system with the proposed NDC.

4. EXPERIMENTAL SETUP AND RESULTS

Several experiments are conducted so as to evaluate the performance of the proposed approaches.

4.1. Experimental Setup and System Parameter

In the following, the experimental hardware and their associated parameters are presented.

4.1.1. Hardware of the experimental system

The hardware of the experimental system is composed of a personal computer, a DSP-based motion control card (equipped with a TI TMS320C32 floating point processor), and a Panasonic AC servomotor with a built-in incremental encoder (2500×4 pulses/rev) for position feedback and velocity estimation. In addition, the motor shaft is attached with a thin circular disk (weight: 537g) which is used as an external load. Note that the drive of the AC servomotor is set to the torque mode throughout the experiments. Moreover, in order to assess the capability in estimating disturbance/load torque, a dynamometer is used to provide the additional disturbance torques. The hardware of the experimental system is illustrated in Fig. 5.

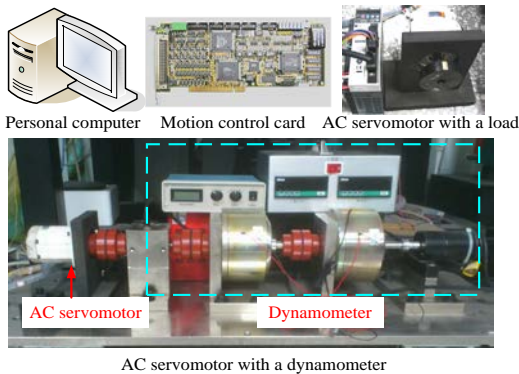


Fig. 5 Hardware of the experimental system used to evaluate the performance of the proposed approach.

4.1.2. Parameter setting of motion control system

The transfer functions for the servomotor connected to an external load (e.g., a thin circular disk) and the servomotor connected to the dynamometer are obtained using the dynamic analyzer Agilent 35670A. Using the obtained plant parameters \hat{J}_m and \hat{B}_m , one can determine appropriate gain constants K_P , K_I in Figs 1-4. In addition, with the desired damping ratio and natural frequency given, the values of gain constants K_1 , K_2 in the PICTO, the PICTOC, and the NDC can also be determined (Tsai et al., 2000; Nise, 2007; Wu et al., 2010). Moreover, the cutoff frequency of the low-pass filter $Q(s)$ is set to 40 Hz in the DOB. In this paper, the identified plant parameters and the selected gain constants for different experiments are summarized in Table 1.

Table 1 Plant parameters and gain constants used in the experiment

Coefficients	Selected parameters	
	Connected to a thin circular disk	Connected to a dynamometer
\hat{J}_m	0.00037386 Nm/(rad/s ²)	0.00089323 Nm/(rad/s ²)
\hat{B}_m	0.00026742 Nm/(rad/s)	0.0038525 Nm/(rad/s)
K_P	0.02	0.02
K_I	0.04	0.04
K_1	0.08	0.15
K_2	0.05	0.35

Furthermore, to facilitate the verification process and also improve the motion accuracy, a friction compensator based on the LuGre friction model (Canudas de Wit et al. 1995) is adopted in the disturbance compensation structure shown in Fig. 6. The LuGre friction model is mathematically expressed as (Canudas de Wit et al., 1995; Kermani et al., 2007):

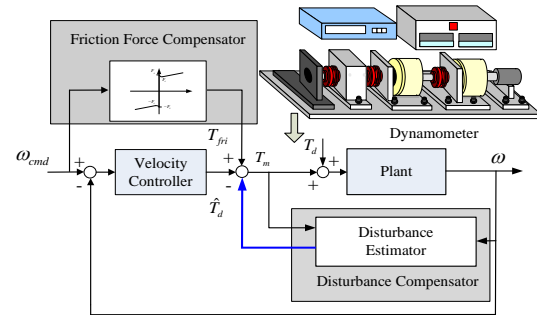


Fig. 6 Control block diagram of the experimental system.

$$F = \sigma_0 z + \sigma_1 \frac{dz}{dt} + \sigma_2 \dot{\theta} \quad (21)$$

$$\frac{dz}{dt} = \dot{\theta} - \sigma_0 \frac{|\dot{\theta}|}{g(\dot{\theta})} z \quad (22)$$

In Eqs. (21) and (22), z is the average deflection of the bristles and $\dot{\theta}$ is the relative velocity between two contact surfaces. Additionally, σ_0 , σ_1 , and σ_2 are the stiffness, damping, and viscous friction coefficients, respectively. $g(\dot{\theta})$ is a nonlinear function used

to describe the Stribeck phenomena, which can be expressed as:

$$g(\dot{\theta}) = F_c + (F_s - F_c)e^{-\alpha|\dot{\theta}|}, \quad (23)$$

where F_c is the Coulomb friction, F_s is the stiction force, and α describes the variation of $g(\dot{\theta})$ between F_s and F_c . In this paper, the identification of the LuGre friction model is mainly based on the approached developed in Kermani et al. (2007). The identification results for the LuGre friction model are listed in Table 2. Table 2 Coefficients of the LuGre friction model for the experimental system

Coefficients	Identification results	
	Connected to a thin circular disk	Connected to a dynamometer
α	0.28684	0.20618
F_c	0.01911 Nm	0.03196 Nm
F_s	0.02137 Nm	0.5109 Nm
σ_0	3.7580 Nm/rad	18.578 Nm/rad
σ_1	0.02481 Nm/(rad/s)	0.05563 Nm/(rad/s)
σ_2	0.00196 Nm/(rad/s)	0.01282 Nm/(rad/s)

Figure 6 shows the control block diagram of the experimental system, where T_{fri} represents the feedforward friction compensation term. Note that the external disturbance torque T_d indicated in Fig.6 is provided by the dynamometer.

4.2. Experimental Results

In order to verify the effectiveness of the proposed approaches, several experiments have been conducted under different test conditions.

4.2.1. Performance evaluation of the proposed NDC

To demonstrate the estimation capability of the proposed approach, in this experiment, three load torque estimation tasks are performed. The first one is to estimate an external constant load torque (0.2 Nm), the second one is to estimate a varying load torque (0.1 Nm~0.3 Nm: $0.2+0.1\sin(2\pi ft)$, where $f=1$ Hz), and the last one is to estimate a frequency varying load torque (0.1 Nm~0.3 Nm: $0.2+0.1\sin(2\pi ft)$, where f is swept from 0.05Hz to 1Hz). All of the external loads are provided by the dynamometer. For all disturbance estimation tasks, four different load torque estimation approaches are used to estimate load torque under a speed control of 600 rpm. The load torque estimation approaches used in the experiment include the PICTO (without disturbance compensation), the DOB (conventional DOB), the PICTOC (PICTO with the disturbance compensation path), and the proposed NDC.

1) Constant load torque estimation

Results of the constant load torque estimation experiment are illustrated in Fig. 7 and listed in Table 3. Figure 7(a) shows the estimated external disturbance load torque (almost equal to 0 Nm) before adding the extra load, while Fig. 7(b) shows the total estimated load torque (almost equal to 0.2 Nm) after

adding a constant load torque (0.2 Nm provided by the dynamometer) to the servomotor. Here, the PICTO is employed to estimate the load torque shown in Figs. 7(a) and 7(b). Figures 7(c), 7(d), and 7(e) show the estimated load torque using the DOB, the PICTOC, and the proposed NDC, respectively.

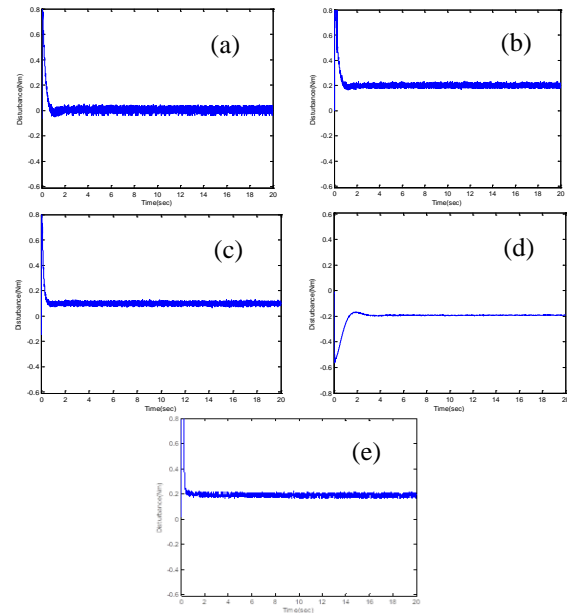


Fig. 7 Experimental results of the constant load torque estimation using different estimation approaches: (a). External disturbance without extra load torque; (b). Total load torque after adding a constant load torque; (c). Estimated load torque obtained using the PICTOC; (d). Estimated load torque obtained using the DOB; (e) Estimated load torque obtained using the proposed NDC.

According to the experimental results, clearly it can be found that the average estimated load torque (≈ 0.2 Nm) obtained from the NDC is almost the same as the servomotor's real load torque (≈ 0.2 Nm, as shown in Fig. 7(b)). However, the average estimated load torque provided by the PICTOC is only half of the real load torque (≈ 0.1 Nm). Table 3 also lists the experimental results in steady state (calculated after 2 seconds) for different disturbance estimation approaches. Obviously, according to results shown in Fig. 7 and Table 3, the proposed NDC exhibits superior estimation ability to the PICTOC and the DOB in constant load torque estimation. Note that the performance indices used in all experimental results are "AIAE", "RMS", and " $\|M\|_{max}$ " where "AIAE" represents the average integral of the absolute error; "RMS" represents the root mean square error, and " $\|M\|_{max}$ " represents the maximum absolute error.

2) Varying load torque estimation

Figure 8 illustrates the experimental results of varying load torque estimation. Figure 8(a) shows the total estimated load torque after adding a varying load ($0.2+0.1\sin(2\pi t)$ provided by the dynamometer) to

the servomotor. Figures 8(b), 8(c), and 8(d) show the estimated load torque obtained using the PICTOC, the DOB, and the proposed NDC, respectively. Based on the experimental results shown in Fig.8, clearly the profile of estimated load torque obtained using the NDC is more similar to the real load torque (as shown in Fig.8(a)) than that obtained by the other two approaches.

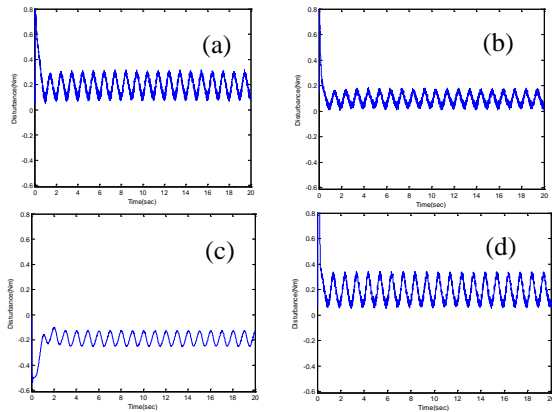


Fig. 8 Experimental results of varying load torque estimation for different estimation approaches: (a) Total load torque after adding a varying load torque; (b) Estimated load torque by the PICTOC; (c) Estimated load torque by the DOB; (d) Estimated load torque by the proposed NDC.

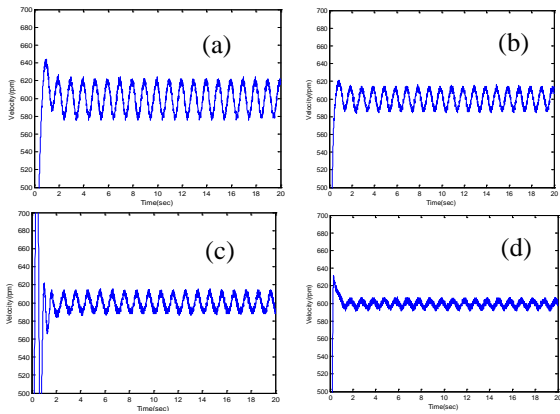


Fig. 9 Velocity profiles of the speed control system consisting of a feedback controller combined with different estimation approaches at 600 rpm (under a varying load torque) (a) With the PICTO; (b) With the PICTOC; (c) With the DOB; (d) With the proposed NDC.

In addition, the resulting velocity profiles are shown in Fig. 9. Figure 9(a) shows the velocity profile of the speed control system consisting of a feedback controller combined with the PICTO; Fig. 9(b) shows the velocity profile of the speed control system consisting of a feedback controller combined with the PICTOC; Fig. 9(c) shows the velocity profile of the speed control system consisting of a feedback controller com-

combined with the DOB; Fig. 9(d) shows the velocity profile of the speed control system consisting of a feedback controller combined with the proposed NDC. According to the experimental results shown in Fig. 9, clearly, the ripple of the velocity profile can be effectively suppressed by the proposed NDC due to the fact that the proposed NDC can accurately estimate the load torque.

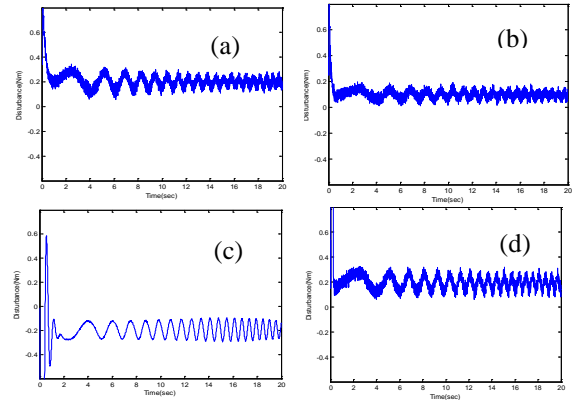


Fig. 10 Experimental results of frequency varying load torque estimation for different estimation approaches: (a) Total load torque after adding a frequency varying load torque; (b) Estimated load torque obtained using the PICTOC; (c) Estimated load torque obtained using the DOB; (d) Estimated load torque obtained using the proposed NDC.

3) Frequency varying load torque estimation

Figure 10 illustrates the experimental results of frequency varying load torque estimation. Figure 10(a) shows the results of total load torque estimation after adding a frequency varying load torque to the servomotor. Figures 10(b), 10(c), and 10(d) show the estimated load torque obtained using the PICTOC, the DOB, and the proposed NDC, respectively. Figure 11 shows the resulting velocity profiles of the speed control system consisting of a feedback controller combined with different external disturbance estimation approaches. The experimental results shown in Fig. 10 reveal that the proposed NDC exhibits its best performance in disturbance estimation. Furthermore, Fig. 11 clearly indicates that the ripple in velocity profile caused by undesirable variable external disturbance can also be effectively suppressed due to the fact that the proposed NDC can accurately estimate the load torque even for the case of frequency varying load torque.

4.2.2. Performance evaluation of the proposed NDC used for low-speed motion control

As previously mentioned, when a servomechanism undergoes a low-speed motion, deterioration in motion accuracy will occur due to friction and/or other disturbances such as external load torque.

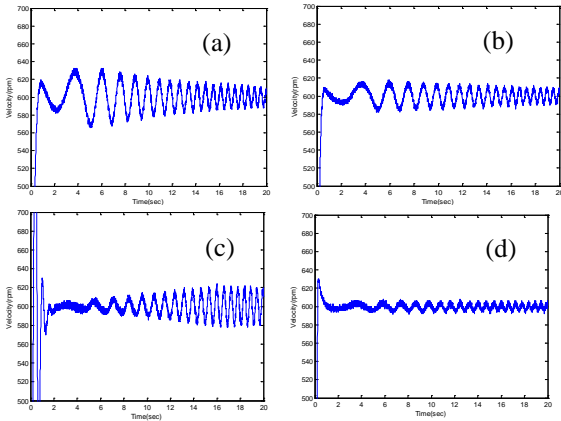


Fig. 11 Velocity profiles of the speed control system consisting of a feedback controller combined with different estimation approaches at 600 rpm (under a frequency varying load torque): (a) With the PICTO; (b) With the PICTOC; (c) With the DOB; (d) With the proposed NDC.

In order to demonstrate the feasibility of the proposed approach when applied to low-speed motion control problems, in this experiment five different motion control structures are used to control the velocity of a servomotor at 60 rpm, 6 rpm, and 1 rpm (a thin circular disk is used as the extra load). The tested speed control structures include: proportional-integral control without friction and disturbance compensation (PI), PI control combined with a LuGre model-based friction compensator (PI+FC), PI control combined with the PICTOC (PI+PICTOC), PI control combined with the DOB (PI+DOB), and the PI control combined with the proposed approach (PI+NDC).

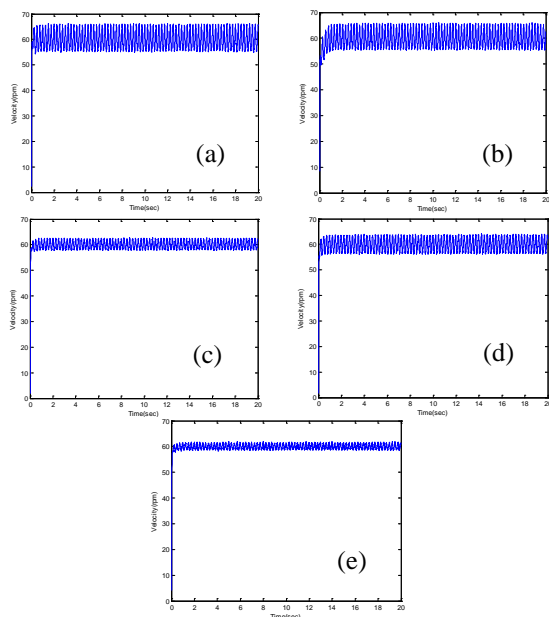


Fig. 12 Experimental results of different speed control structures at 60 rpm: (a). PI; (b). PI+FC; (c). PI+PICTOC; (d).PI+DOB; (e). PI+NDC.

Experimental results of different speed control structures at 60 rpm, 6 rpm, and 1 rpm are shown in

Figs. 12, 13 and 14, respectively. Figures 12(a), 13(a), and 14(a) show the velocity profiles obtained using the PI, Figs. 12(b), 13(b), and 14(b) show the velocity profiles obtained using the PI+FC, Figs. 12(c), 13(c), and 14(c) show the velocity profiles obtained using the PI+PICTOC, Figs. 12(d), 13(d), and 14(d) show the velocity profiles obtained using the PI+DOB, while Figs. 12(e), 13(e), and 14(e) show the velocity profiles obtained using the proposed approach PI+NDC.

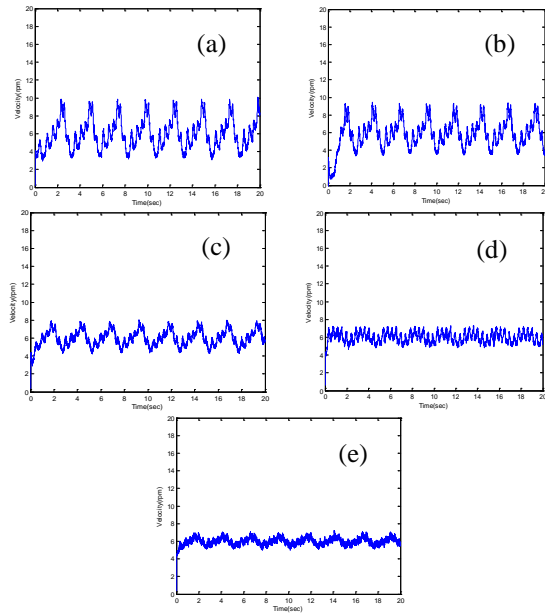


Fig. 13 Experimental results of different speed control structures at 6 rpm: (a). PI; (b). PI+FC; (c). PI+PICTOC; (d).PI+DOB; (e). PI+NDC.

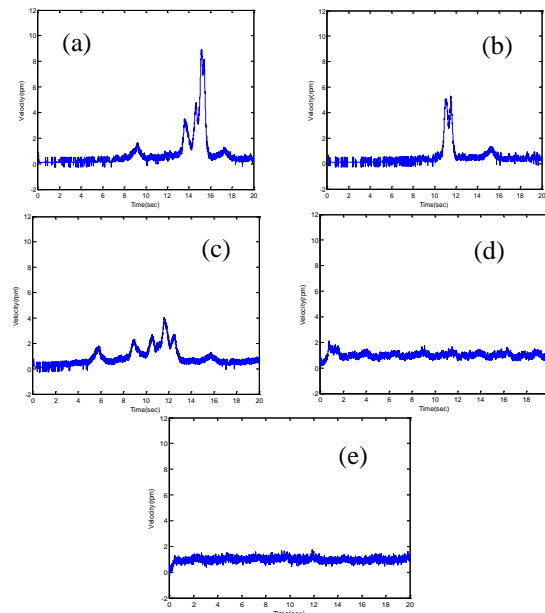


Fig. 14 Experimental results of different speed control structures at 1 rpm: (a). PI; (b). PI+FC; (c). PI+PICTOC; (d).PI+DOB; (e). PI+NDC.

Table 3 Performance comparison for different external disturbance estimation approaches

Loaded with a constant torque: 0.2 Nm	AIAE(Nm)	RMS(Nm)
PICTO (original torque, without loaded)	0.0112	0.0154
PICTO	0.1995	0.1998
PICTOC	0.0978	0.0984
DOB	0.1905	0.1906
NDC	0.1924	0.1927

Table 4 Performance comparisons among different speed control structures

Experimental Results Definitions	Performance index of velocity errors (rpm)		
	AIAE	RMS	$\ M\ _{\max}$
60 rpm			
PI	3.1771	3.5605	6.2300
PI+FC	2.9918	3.3543	6.0370
PI+PICTOC	1.3324	1.4977	2.7390
PI+DOB	2.2418	2.5026	4.1310
PI+ NDC	0.7604	0.8581	1.9020
6 rpm			
PI	1.3485	1.6712	4.1150
PI+FC	1.1293	1.4114	3.4360
PI+PICTOC	0.6912	0.8428	2.0670
PI+DOB	0.4279	0.5298	1.3360
PI+ NDC	0.3154	0.3903	1.2200
1 rpm			
PI	0.8992	1.3974	7.9610
PI+FC	0.8086	0.9796	4.3040
PI+PICTOC	0.5971	0.7323	3.0500
PI+DOB	0.1934	0.2314	0.7390
PI+ NDC	0.1553	0.1924	0.7340

Table 4 lists the experimental results for different speed control structures. According to the results shown in Figs. 12-14, and Table 4, obviously, the proposed approach exhibits the best performance among all the tested speed control structures. In particular, when the servomotor is operated at a relatively low-speed motion of 1 rpm, the proposed approach can cope with the stick-slip phenomena due to the inherent friction force or external disturbance and also effectively suppress the noise effects.

5. CONCLUSIONS

In this paper, a novel disturbance estimation /compensation approach is proposed for motion control accuracy improvement. First, in order to evaluate the disturbance torque estimation ability of the proposed approach, theoretical analysis of the transfer functions for different estimation structures are performed. Subsequently, several experiments on load torque estimation/compensation of speed control systems are then conducted to evaluate the performance of the proposed approach. The main contribution of the proposed NDC is that it can effectively estimate and compensate for the

disturbance/load torque simultaneously even for the case of a relatively low-speed motion or under a frequency varying load torque. Experimental results verify the effectiveness of the proposed NDC.

ACKNOWLEDGMENTS

The authors would like to thank the National Science Council of Republic of China for support of this research under Grants No. MOST 103-2221-E-415-031- and No. MOST 110-2221-E-224-053-. In particular, the authors would like to thank Mr. P.-Y. Huang for his great assistance with this work.

REFERENCES

- Su, K. H. & Cheng, M. Y. (2008) Contouring accuracy improvement using cross -coupled control and position error compensator. *International Journal of Machine Tools and Manufacture*, 48, 1444–1453.
- Tomizuka, M. (1993) On the design of digital tracking controllers. *ASME Journal of Dynamic Systems, Measurement, and Control*, 115, 412–418.
- Targ, Y. S. & Cheng, H. E. (1995) An investigation of Stick-Slip friction on the contouring accuracy of CNC machine tools. *International Journal of Machine Tools and Manufacture*, 35, 565-576.
- Karnopp, D. (1985) Computer simulation of Slip-Stick friction in mechanical dynamic systems. *ASME Journal of Dynamic Systems, Measurement, and Control*, 107, 100-103.
- Canudas de Wit, C., Olson, H., Åström, K. J. & Lischinsky, P. (1995) A new model for control of systems with friction. *IEEE Transactions on Automatic Control*, 40, 419-425.
- Ohishi, K., Nakao, M., Ohnishi, K., & Miyach, K. (1987) Microprocessor -controlled dc motor for load-insensitive position servo system. *IEEE Transactions on Industrial Electronics*, IE-34, 44–49.
- Ko, J. S., Lee, J. H., Chung, S. K., & Youn, M. J. (1993) A robust digital position control of brushless dc motor with dead beat load torque observer. *IEEE Transactions on Industrial Electronics*, 40, 512–520.
- Umeno, T., & Hori, T. (1991) Robust speed control of DC servomotors using modern two degrees-of-freedom controller design. *IEEE Transactions on Industrial Electronics*, 38, 363-368.
- Choi, B. K., Choi, C. H., & Lim, H. (1999) Model-based disturbance attenuation for CNC machining centers in cutting process. *IEEE/ASME Transactions on Mechatronics*, 4, 157–168.
- Tsai, M. C., Tseng, E. C., & Cheng, M. Y. (2000) Design of a torque observer for detecting abnormal load. *Control Engineering Practice*, 8, 259-269.
- Lee, H. S., & Tomizuka, M. (1996) Robust motion

- controller design for high-accuracy positioning systems,” IEEE Transactions on Industrial Electronics, 43, 48-55.
- Kobayashi, H., Katsura, S., & Ohnishi, K. (2007) An analysis of parameter variations of disturbance observer for motion control, IEEE Transactions on Industrial Electronics, 54, 3413-3421.
- Lu, Y. S. (2008) Smooth speed control of motor drives with asymptotic disturbance compensation. Control Engineering Practice, 16, 597-608.
- Yao, B., Al-Majed, M., & Tomizuka, M. (1997) High-performance robust motion control of machine tools: An adaptive robust control approach and comparative experiments. IEEE/ASME Transactions on Mechatronics, 2, 63-76.
- Kim, B. K., & Chung, W. K. (2003) Advanced disturbance observer design for mechanical positioning systems. IEEE Transactions on Industrial Electronics, 50, 1207-1216.
- Xie, W (2010) High frequency measurement noise rejection based on disturbance observer. Journal of the Franklin Institute, 347, 1825-1836.
- Shao, K., Zheng, J., Wang, H., Xu, F., Wang, X., & Liang, B., (2021) Recursive sliding mode control with adaptive disturbance observer for a linear motor positioner. Mechanical Systems and Signal Processing, 146, 1-16.
- Sariyildiz E., Oboe R., & Ohnishi K., (2020) Disturbance Observer-based Robust Control and Its Applications: 35th Anniversary Overview. IEEE Trans. on Ind. Electronics, 67, 2042-2053.
- Nise, N. S. (2007) Control systems engineering. (5th ed) New York, John Wiley and Sons.
- Wu, J. C., Su, K. H., & Cheng, M. Y. (2010) Friction and disturbance compensation for speed control of servo control systems. In Proceedings of the 36th annual conference on IEEE industrial electronics (IECON), Glendale, AZ, USA (pp. 1890-1895).
- Kermani, M. R., Patel, R. V., & Moallem, M. (2007) Friction identification and compensation in robotic manipulators. IEEE Transactions on Instrumentation and Measurement, 56, 2346-2353.

干擾量補償法於速度控制 效能改善之分析與研發

蘇科翰

國立雲林科技大學電機工程系

鄭銘揚 吳仁哲

國立成功大學電機工程學系

摘要

於高精度運動控制應用中，消除摩擦力及外部干擾之影響為重要的研究課題之一。特別於低速度下或反轉運動時，系統既有之摩擦力及外部干擾量等對運動控制精度往往有著極大的影響。為能提升運動控制精度，本論文提出一種干擾量補償機制，為以系統模型為基礎發展之干擾量補償器(NDC)。其特點為非但可精確地估測出外部干擾量與負載力矩外，同時並具備可抑制外部干擾量並降低量測雜訊之優點。本論文中，為先以理論分析各種不同方法之轉移函數，並進而透過估測負載力矩、低速度控制等各種實驗來驗證本論文所提出之方法相較於其他架構確實可以有效地提升運動控制精度。